Japanese Journal of Radiology (2021) 39:101–117
https://doi.org/10.1007/s11604-020-01031-2

INVITED REVIEW

Anterior mediastinal lesions: CT and MRI features and differential diagnosis

Takahiko Nakazono[1] · Ken Yamaguchi[1] · Ryoko Egashira[1] · Masanobu Mizuguchi[1] · Hiroyuki Irie[1]

Received: 4 July 2020 / Accepted: 11 August 2020 / Published online: 2 September 2020

Abstract
Anterior mediastinum is the most common location of mediastinal tumors, which include various solid and cystic lesions. The lesion location and CT and MRI features are important in the differential diagnosis. Recently, CT-based mediastinal compartment classification systems were proposed and suggested to be useful for accurate evaluation of mediastinal lesions. CT and MRI reflect the pathological findings of mediastinal lesions, and knowledge of the pathological features is important for the differential diagnosis. In this article, we review the CT and MRI features of anterior mediastinal lesions and describe important points in the differential diagnosis.

Keywords Mediastinum · Anterior · Computed tomography · Magnetic resonance imaging

Introduction

Various solid and cystic lesions occur in the mediastinum. The location and imaging features are important for the differential diagnosis of these lesions. There are several traditional mediastinal compartment classifications based on anatomy [1] and chest radiographs [2]. However, some mediastinal lesions cannot be reliably localized to a specific compartment, since considerable overlap exists among the radiographically imaged compartments. Mediastinal lesions are optimally evaluated with cross-sectional imaging techniques such as computed tomography (CT) and magnetic resonance imaging (MRI). Accordingly, new CT-based mediastinal compartment classification systems were recently proposed and were suggested to be useful for accurate evaluation of location of mediastinal lesions [3, 4]. CT and MRI reflect histopathological features of mediastinal lesions. MRI may provide additional information to the CT findings of mediastinal lesions. In this article, we review CT and MRI features of anterior mediastinal lesions according to the CT-based mediastinal compartment classification systems.

✉ Takahiko Nakazono
nakazot@cc.saga-u.ac.jp

[1] Department of Radiology, Faculty of Medicine, Saga University, Nabeshima 5-1-1, Saga City, Saga 849-8501, Japan

CT-based mediastinal compartment classification systems

The Japanese Association of Research of the Thymus (JART) proposed a CT-based 4-compartment mediastinal classification system that included the superior portion of the mediastinum, anterior mediastinum (prevascular zone), middle mediastinum (peritracheoesophageal zone), and posterior mediastinum (paravertebral zone) (Fig. 1a) [3]. The inferior boundary of the superior portion of the mediastinum is a horizontal plane at the intersection of the caudal margin of the brachiocephalic vein with the trachea [3]. Classifying the superior portion of the mediastinum has the advantage of making it easy to differentiate an intrathoracic goiter or neurogenic tumor of the thoracic inlet from other mediastinal tumors. The lateral boundaries of the anterior mediastinum are the parietal (mediastinal) pleural reflections (including the lateral rims of the bilateral internal thoracic arteries and veins, and the superior and inferior pulmonary veins). The posterior boundary of the anterior mediastinum is formed by the pericardium, anterior rims of the left brachiocephalic vein, superior vena cava, superior and inferior pulmonary veins, ascending aorta, and lateral rim of the aortic arch (Fig. 1a) [3]. The International Thymic Malignancy Interest Group (ITMIG) modified and simplified the JART classification to produce a CT-based 3-compartment classification that has the advantages of similarity to the published

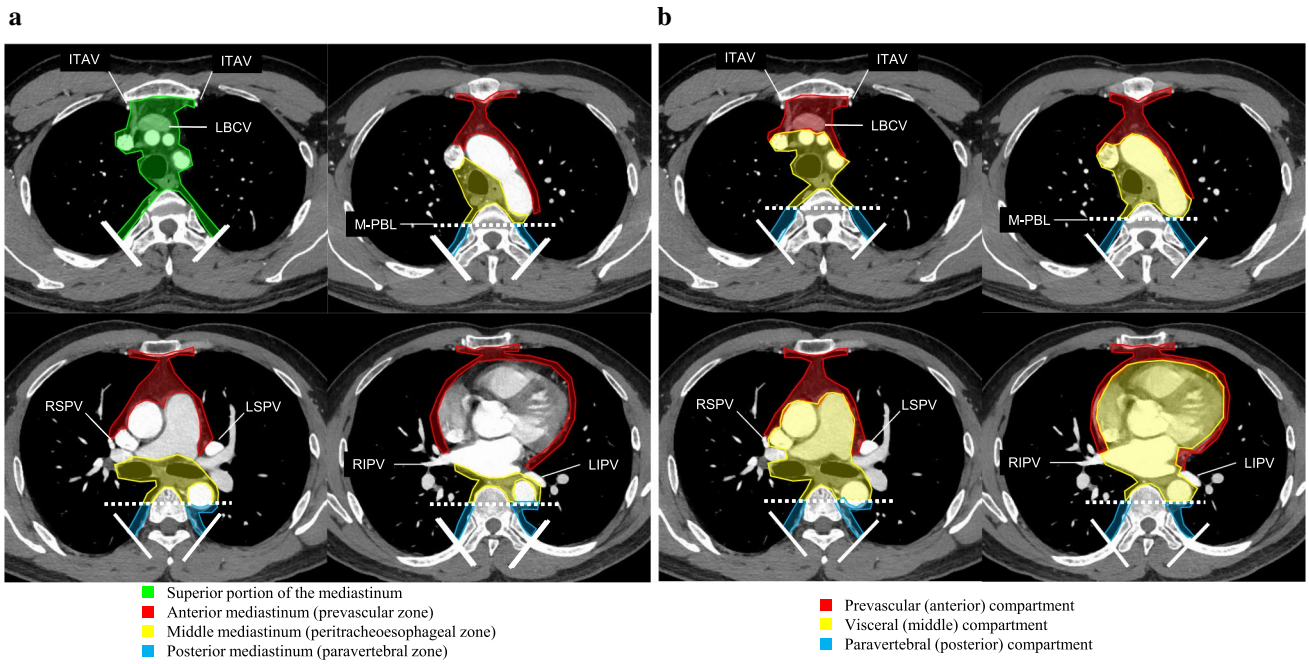

Fig. 1 **a** Axial contrast-enhanced CT images representing the JART CT-based mediastinal compartment classification [3]. The superior portion of the mediastinum is the compartment between the thoracic inlet and the horizontal plane at the intersection of the caudate margin of the brachiocephalic vein with the trachea. The heart and great vessels in the pericardium are not included in the middle mediastinum on the JART classification. **b** Axial contrast-enhanced CT images representing the ITMIG CT-based mediastinal compartment classification [4]. The ITMIG simplified the JART classification and omitted the superior portion of the mediastinum. The visceral compartment of the ITIMG classification includes the heart and great vessels in the pericardium. *LBCV* left brachiocephalic vein, *ITAV* internal thoracic arteries and vein, *RSPV* right superior pulmonary vein, *LSPV* left superior pulmonary vein, *RIPV* right inferior pulmonary vein, *LIPV* left inferior pulmonary vein, *M-PBL* middle-posterior boundary line, *V-PBL* visceral-paravertebral compartment boundary line (a vertical line connecting a point on each thoracic vertebral body at 1 cm behind its anterior margin)

anatomic, clinical, and radiologic 3-compartment models currently used, a less complicated design, and the use of true anatomic planes to establish compartmental boundaries [4]. The ITMIG CT-based classification includes the prevascular (anterior), visceral (middle), and paravertebral (posterior) compartments (Fig. 1b) [4]. The posterior boundary of the prevascular compartment is the anterior aspect of the pericardium as it wraps around in a curvilinear fashion. Based on these landmarks, the major contents of the prevascular compartment include the thymus, fat, lymph nodes, and left brachiocephalic vein (Fig. 1b) [4]. In the ITMIG classification, the heart and great vessels are included in the visceral (middle) compartment (Fig. 1b) [4]. In contrast, the heart and great vessels are not included in the middle mediastinum in the JART classification (Fig. 1a) [3]. Table 1 shows the differential diagnosis of solid and cystic anterior mediastinal lesions according to the ITMIG CT-based mediastinal compartment classification system. Lesion location and imaging features are key to the differential diagnosis of mediastinal lesions.

Imaging features of solid anterior mediastinal lesions

Solid anterior mediastinal lesions include thymic epithelial tumors, thymic neuroendocrine tumors (NETs), malignant lymphomas, germ cell tumors (GCTs), thymic hyperplasia, and thymolipoma. Intrathoracic goiter may extend to the superior portion of the mediastinum (JART), anterior mediastinum, and middle mediastinum. Ectopic parathyroid adenomas commonly occur in the superior portion of the mediastinum and anterior mediastinum. Peripheral nerve sheath tumors arising from the vagus nerves and phrenic nerves rarely occur in the superior portion of the mediastinum and anterior mediastinum.

On imaging evaluation of solid mediastinal lesions, such features as the lesion shape, margin, invasion to the surrounding structures, peripheral capsule, septum, calcification, fat, cystic change, necrosis, and hemorrhage in the lesion are important. MRI is superior to CT for evaluating

Table 1 Differential diagnoses and imaging features of anterior mediastinal lesions

	Differential diagnoses	Age and gender predilections of the patients	Imaging features
Solid	Thymomas	50–60 years; no gender predilection	Low-risk: round or oval shape; smooth contour; almost complete capsule, septa High-risk: irregular contour; pleural dissemination
	Thymic carcinomas	50 years; male	Invasive; lymphogenous and hematogenous metastases
	Thymic neuroendocrine tumors	40–50 years; male	Carcinoid: hypervascular LCNEC, small cell carcinoma: lymphogenous and hematogenous metastases
	Malignant lymphomas	PMBCL: 20–30 years; female NSHL: 10–30 years or 50 years; female T-LBL: 10–20 years; male	Lymph node enlargements; low ADC value
	Germ cell tumors	20–30 years; almost exclusively male	Seminoma: limited necrosis NSGCTs: marked hemorrhagic necrosis; lymphogenous and hematogenous metastases
	Thymic hyperplasia	Any age; no gender predilection	Flat triangular shape; intervening fat tissue in the thymic tissue
	Thymolipoma	20 years; no gender predilection	Large and soft mass; intermingled fat tissue and soft tissue
	Intrathoracic goiter	Adults; female	High attenuation on plain CT; hypervascular; calcification; cystic change
	Ectopic parathyroid adenoma	Any age; no gender predilection	Hypervascular small nodule
	Peripheral nerve tumors	20–30 years; no gender predilection	Mass along the route of the phrenic or vagus nerves; target sign
	Paraganglioma	30–40 years, no gender predilection	Adjacent to the great vessels; hypervascular; hemorrhagic necrosis
Cystic	Thymic cysts	Any age; no gender predilection	Congenital: unilocular; thin wall Acquired: multilocular; thick wall and septa; serous, viscous, or hemorrhagic fluid
	MALT lymphoma	50–60 years; female	Multilocular; thick wall and septa; mixture of solid and cystic components
	Pericardial cyst	30–40 years; no gender predilection	Unilocular; thin wall
	Mature cystic teratoma	Children and young adults; no gender predilection	Unilocular or multilocular; fat and calcification; thick wall and septa; viscous fluid
	Cystic lymphangioma	Young children; no gender predilection	Multilocular, thin wall and septa
	Thyroid cyst	Any age; no gender predilection	Cystic change in intrathoracic goiter
	Parathyroid cyst	Any age; no gender predilection	Unilocular; thin wall
	Neurogenic tumors with cystic change	20–30 years; no gender predilection	Thick wall and/or solid component

LCNEC large cell neuroendocrine carcinoma, *PMBCL* primary mediastinal large B-cell lymphoma, *NSHL* nodular sclerosis Hodgkin lymphoma, *T-LBL* T-cell lymphoblastic lymphoma, *ADC* apparent diffusion coefficient, *NSGCTs* nonseminomatous germ cell tumors, *MALT* mucosa-associated lymphoid tissue

of the capsule, septum, fat, and hemorrhage in the lesion. Diffusion-weighted images (DWIs) have been reported to reflect tumor cellularity and be useful for differentiation between benign and malignant mediastinal tumors [5]. MRI can provide additional information to augment the CT findings of mediastinal lesions.

Thymic epithelial tumors

Thymomas occur at almost all ages, with a peak incidence at 55–65 years, and are associated with various autoimmune diseases such as myasthenia gravis (MG) [6]. The

2015 World Health Organization (WHO) Classification of Tumors of the Thymus has histologically classified thymomas into types A, AB, B1, B2 and B3 [6]. Types A, AB, and B1 are reported to be low risk, while types B2 and B3 are high risk. High-risk thymomas frequently show extracapsular invasion, and their prognosis is worse than that of low-risk thymomas. Thymic carcinomas usually present at around 50 years of age. Thymic NETs are separately categorized from other thymic carcinomas without neuroendocrine features. Various histological subtypes of thymic carcinoma are included in the WHO classification, with the most common being squamous cell carcinoma [6].

Low-risk thymomas are likely to show a smooth contour on CT and MRI [7, 8] and a low-signal-intensity complete capsule in the periphery of the mass on T2-weighted images (Fig. 2a) [7]. Cystic change, hemorrhage, and low-signal-intensity septa on T2-weighted images are common in thymomas [7]. High-risk thymomas are likely to show an irregular contour [7, 8], and the capsule and septa are more likely to be ill-defined compared to those of low-risk thymomas (Fig. 3) [7]. Calcification is frequent in types B1, B2, and B3 thymomas [8]. Linear or curvilinear calcifications along septa in thymomas are characteristic (Fig. 3a). Pleural dissemination is frequent in high-risk thymomas. Thymic carcinomas are likely to be irregular, invasive, and heterogeneous due to tumor necrosis (Fig. 4) [7, 8]. Lymph node and hematogenous metastases (Fig. 4) are common in thymic carcinomas and rare in thymomas [7, 8]. In a study of dynamic contrast-enhanced MRI [9], non-invasive thymomas were likely to show early rapid enhancement and washout of the contrast media on delayed phase (Fig. 2d, e). Invasive thymomas and thymic carcinomas were reported to show gradual enhancement, which might reflect abundant fibrous tissues in the tumors (Fig. 3e, f) [9]. In studies on DWI of thymic epithelial tumors, the apparent diffusion coefficient (ADC) values of high-risk thymomas (Fig. 3d) and thymic carcinomas were reported to be lower than those of low-risk thymomas (Fig. 2c) [10], and the ADC values of advanced stage (Masaoka-Koga stage III and IV) thymomas (Fig. 3d) are reported to be lower than those of early stage (Masaoka-Koga stage I and II) thymomas (Fig. 2c) [10, 11].

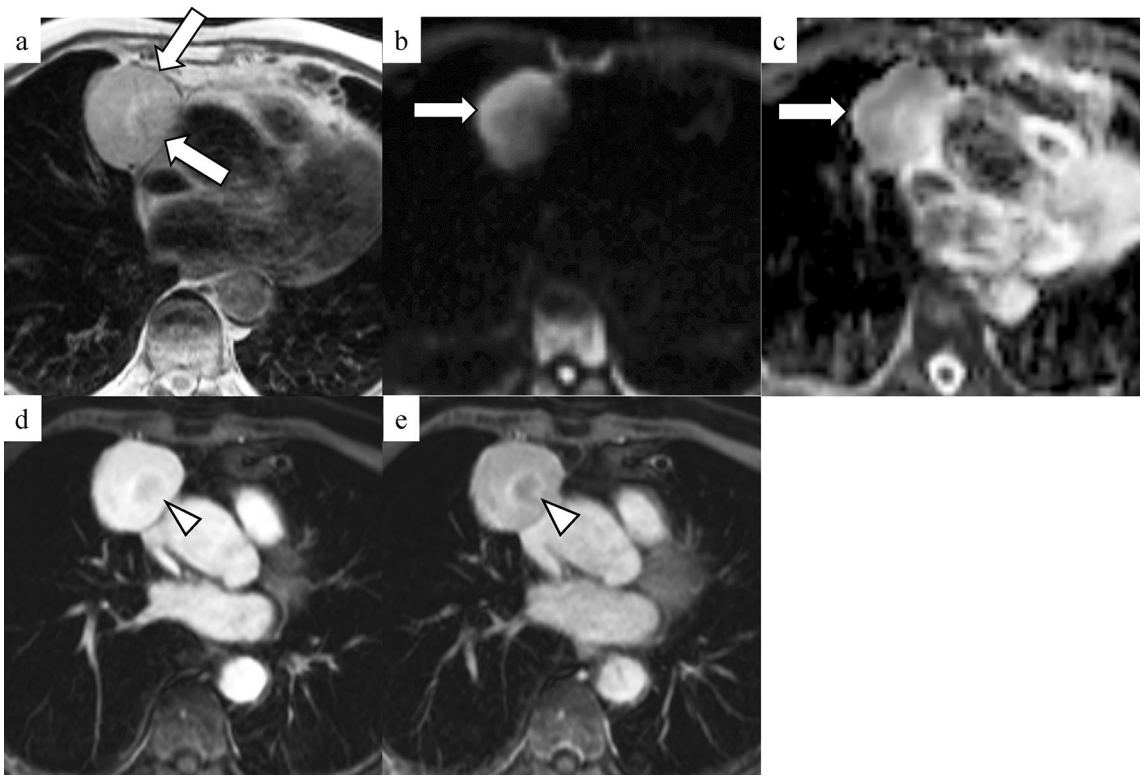

Fig. 2 Low-risk (type AB) thymoma in an 84-year-old woman (Masaoka-Koga clinical stage I) **a** An axial T2-weighted image shows a well-circumscribed round mass with a low-signal-intensity peripheral capsule (arrows) in the anterior mediastinum. **b** An axial diffusion-weighted image ($b = 1000$ s/mm^2) shows high signal intensity of the mass (arrow). **c** The mean ADC value within the mass (arrow) was 1.75×10^{-3} mm^2/s on the ADC map. **d**, **e** Axial dynamic contrast-enhanced MR images (**d** 60 s; **e** 180 s after the start of injection of the contrast material) show a rapid heterogeneous enhancement on the early phase and wash out of the contrast material on the delayed phase in the mass. Central necrosis (arrowheads) is suspected in the mass

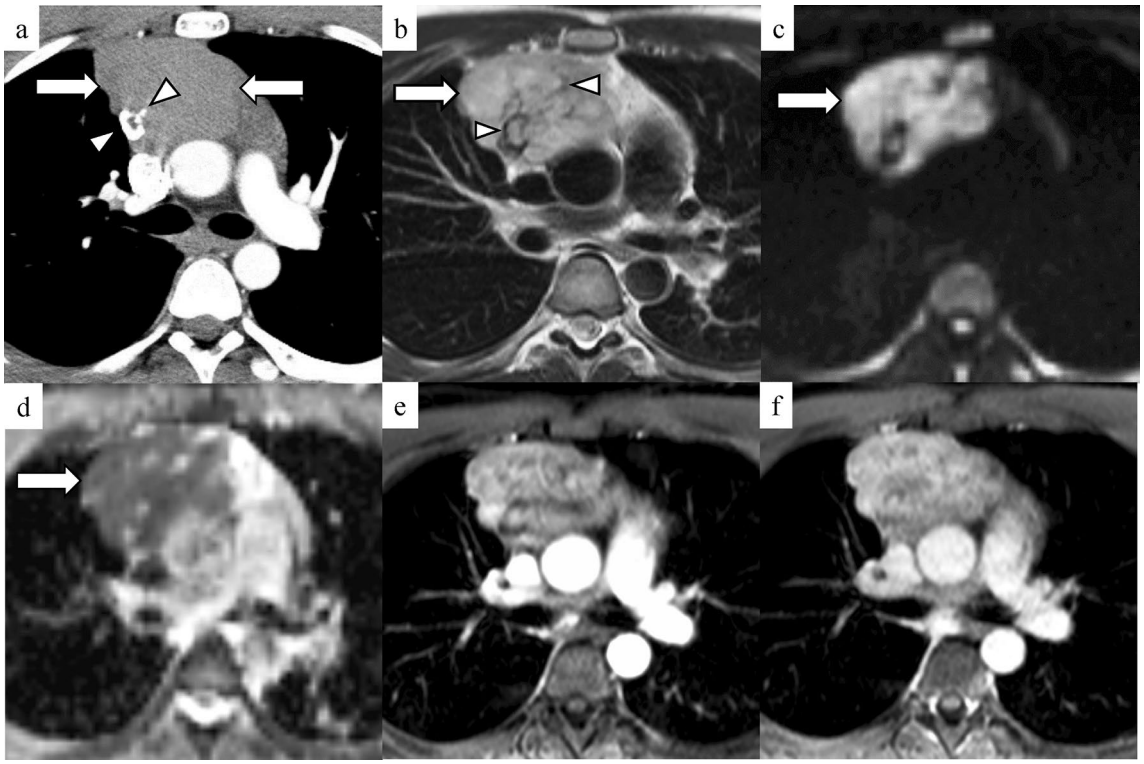

Fig. 3 High-risk (type B2) thymoma in a 24-year-old man (Masaoka-Koga clinical stage III) **a** An axial contrast-enhanced CT image (arterial phase) shows a large mass with an irregular margin (arrows) in the anterior mediastinum. Small or ring-like calcifications (arrowheads) are seen in the mass. A capsule and septum are not seen. **b** An axial T2-weighted image shows heterogeneous high signal intensity of the mass (arrow). Low-signal-intensity septa and calcifications (arrowheads) are seen in the mass. A peripheral capsule is not seen. **c** An axial diffusion-weighted image ($b = 1000$ s/mm^2) shows high signal intensity of the mass (arrow). **d** The mean ADC value within the mass (arrow) was 1.1×10^{-3} mm^2/s on the ADC map. **e**, **f** Axial dynamic contrast-enhanced MR images (**e** 60 s; **f** 180 s after the start of injection of the contrast material) show a gradual heterogeneous enhancement of the mass. Tumor invasion to the left innominate vein was confirmed by the surgery

Thymic neuroendocrine tumors

Thymic NETs are classified into typical carcinoid, atypical carcinoid, large cell neuroendocrine carcinoma (LCNEC), and small cell carcinoma in the WHO classification [6]. The majority of thymic NETs are atypical carcinoids, which usually present at 40–50 years of age [6]. Twenty five percent of thymic carcinoids are associated with multiple endocrine neoplasia (MEN) type 1. Carcinoid syndrome is rare (less than 1% of cases), and Cushing syndrome due to secreting adrenocorticotropic hormone (ACTH) is seen in 17–30% of adult cases of thymic carcinoid [6]. Prognosis is poor in LCNECs and small cell carcinomas [6]. Thymic carcinoids are reported to show a large irregular mass, and a capsule and septum are rarely seen [12]. Necrosis and cystic change are frequent, and the mass is heterogeneous on CT and MRI (Fig. 5). Calcification and hemorrhage may be seen. Because carcinoids are hypervascular, contrast-enhanced CT and MRI show moderate to marked enhancement, and feeding vessels and flow voids may be seen within or around the lesion (Fig. 5) [12]. Recurrence and metastasis in the mediastinum, lymph nodes, lung, and other locations are common in thymic atypical carcinoids, LCNECs, and small cell carcinomas [6].

Malignant lymphomas

Primary mediastinal malignant lymphomas commonly occur in the anterior mediastinum. Major histologic subtypes are primary mediastinal large B-cell lymphoma (PMBCL), nodular sclerosis Hodgkin lymphoma (NSHL), and T-cell lymphoblastic lymphoma (T-LBL) [6]. PMBCLs occur in younger adults with a peak incidence at 20–30 years [6]. PMBCLs show a large irregular or lobulated mass without a peripheral capsule (Fig. 6) [13]. The lesions commonly invade adjacent mediastinal structures such as vessels, chest wall, and lung [14]. Necrosis, cystic change and hemorrhage in the lesion, and mediastinal lymph node enlargement are common (Fig. 6) [14]. Pleural and pericardial effusion are seen in about half of cases [14]. NSHLs are common in young females [6]. NSHLs typically show a lobulated or

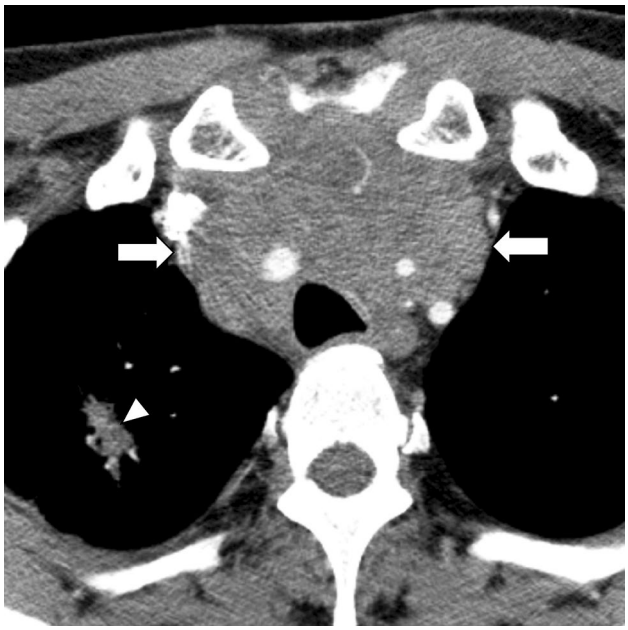

Fig. 4 Thymic carcinoma (lymphoepithelioma-like carcinoma) in a 50-year-old man. An axial contrast-enhanced axial CT image (arterial phase) shows an ill-defined mass (arrows) in the superior portion of the mediastinum and anterior mediastinum. The innominate artery and left common carotid artery are surrounded by the mass, and the trachea and right innominate vein are compressed by the mass. An irregular nodule suspected of being a metastasis (arrowhead) is seen in the upper lobe of the right lung

multinodular mass with limited necrosis and cystic change [13]. Fibrous septa may be seen in the mass, and the peripheral capsule is unclear. Lymph node enlargement may be seen in regions adjacent to the primary lesion [13]. Pleural and pericardial effusion are not frequent [14]. T-LBLs occur in children and young adults with a male predilection [6]. T-LBL patients may complain of chest pain and dyspnea due to rapid enlargement of the mediastinal lesion [6]. T-LBLs show a large heterogenous mass with necrosis (Fig. 7a). Pleural and pericardial effusion are seen in about half of cases [14]. T-LBLs have a predilection for rapid dissemination and the tumor spreads to the extrathoracic lymph nodes (Fig. 7), bone marrow, and central nervous system in extensive disease [14]. In malignant lymphomas, penetration of vessels may be seen (Fig. 7a), and calcification is very rare prior to chemotherapy. Dynamic contrast-enhanced MRI has been reported to show gradual enhancement in malignant lymphomas (Fig. 6d, e) [15]. The ADC values of malignant lymphomas are reported to be very low, reflecting the high cellularity in the tumor (Fig. 6c) [5, 16].

Germ cell tumors

In the WHO classification, mediastinal GCTs are classified to seminoma, embryonal carcinoma, yolk sac tumor, choriocarcinoma, mixed GCT, GCT with somatic-type malignancy, and GCT associated with hematological malignancy [6]. More than 80% of GCTs are benign, with a large majority being mature teratomas. Mature teratomas occur with equal frequency in men and women, while malignant GCTs have a predominant distribution in males during the second to fourth decades. Teratomas account for 58%, and yolk sac tumors make up 42% of mediastinal GCTs in prepubertal male and female patients [6]. Teratomas make up 35%, seminomas 32%, and mixed GCTs 16% of mediastinal GCTs in postpubertal males [6], and teratomas make up 93% of mediastinal GCTs in postpubertal females [6]. Prognosis is worse in nonseminomatous GCTs than in pure seminomas. Seminomas typically show a lobulated or irregular mass. Fibrous septa may be seen in the mass, and a peripheral capsule is not seen (Fig. 8a). Seminomas are relatively homogeneous due to the limited areas of necrosis and hemorrhage in the tumor (Fig. 8) [17]. Contrast-enhanced CT and MRI show

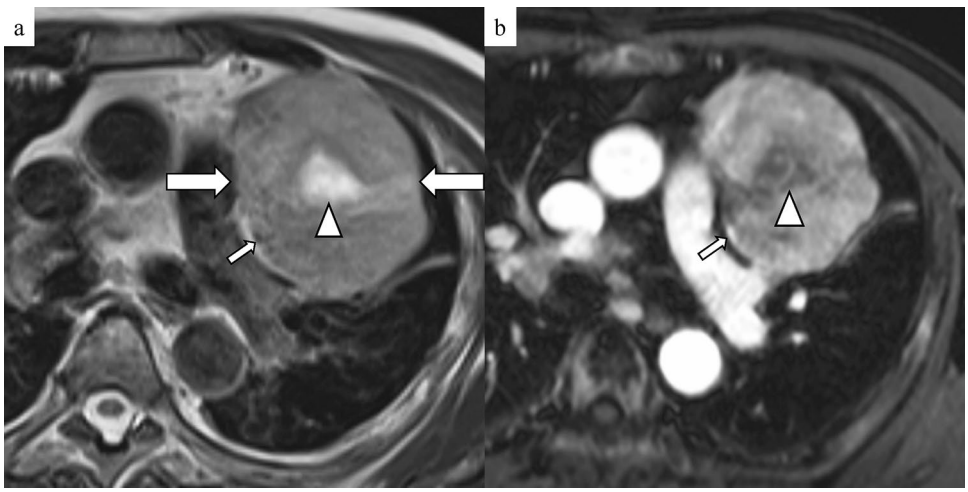

Fig. 5 Thymic atypical carcinoid in a 58-year-old man. **a** An axial T2-weighted image shows a well-circumscribed oval mass (large arrows) in the anterior mediastinum. Central necrosis (arrowhead) and a peripheral flow void (small arrow) are seen in the mass. **b** An axial dynamic contrast-enhanced MR image (30 s after the start of injection of the contrast material) shows rapid heterogeneous enhancement in the mass. Enhancement is not seen in the central necrosis (arrowhead). A feeding vessel (small arrow) is seen in the periphery

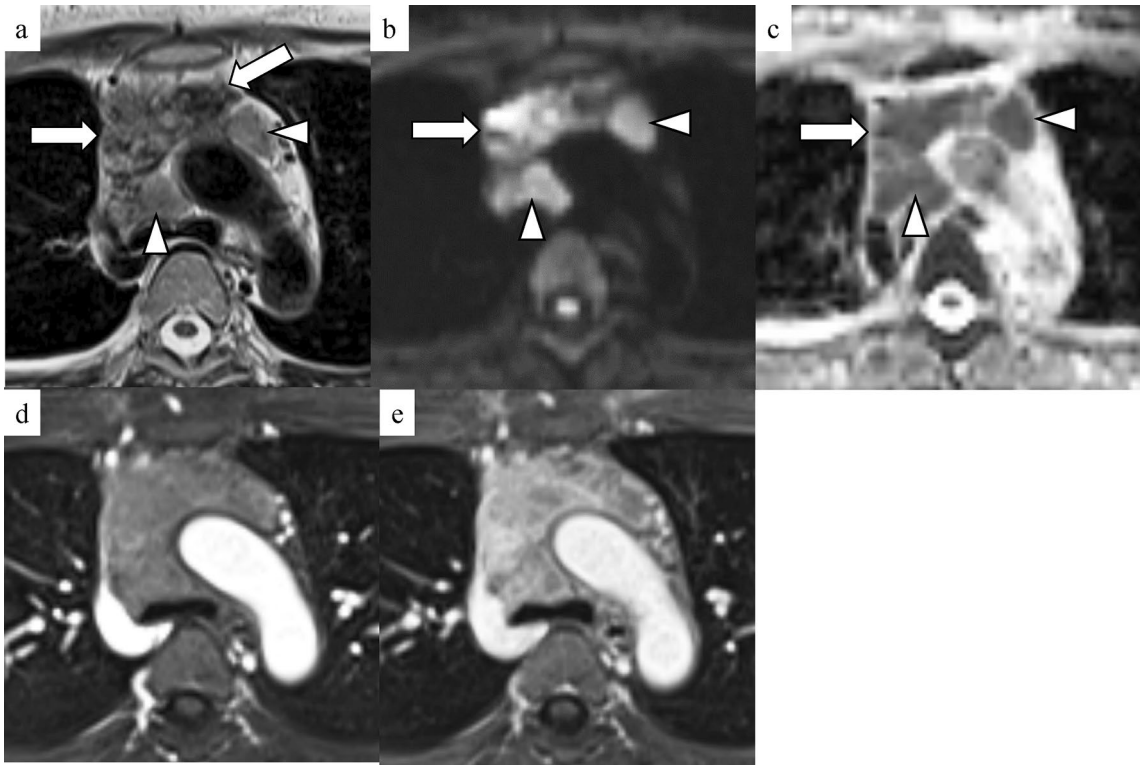

Fig. 6 Primary mediastinal large B-cell lymphoma in a 49-year-old woman. **a** An axial T2-weighted image shows a heterogeneous mass with an irregular margin (arrows) in the anterior mediastinum. A peripheral capsule is not seen. Mediastinal lymph node enlargements (arrowheads) are seen adjacent to the mass. **b** An axial diffusion-weighted image ($b = 1000$ s/mm^2) shows heterogeneous high signal intensity of the mass (arrow) and lymph node enlargements (arrowheads). **c** An axial ADC map shows low ADC values within the mass (arrow; mean ADC value: 0.8×10^{-3} mm^2/s) and lymph node enlargements (arrowheads). **d**, **e** Axial dynamic contrast-enhanced MR images (**d** 60 s; **e** 180 s after the start of injection of the contrast material) show a gradual heterogeneous enhancement of the mass and lymph node enlargements

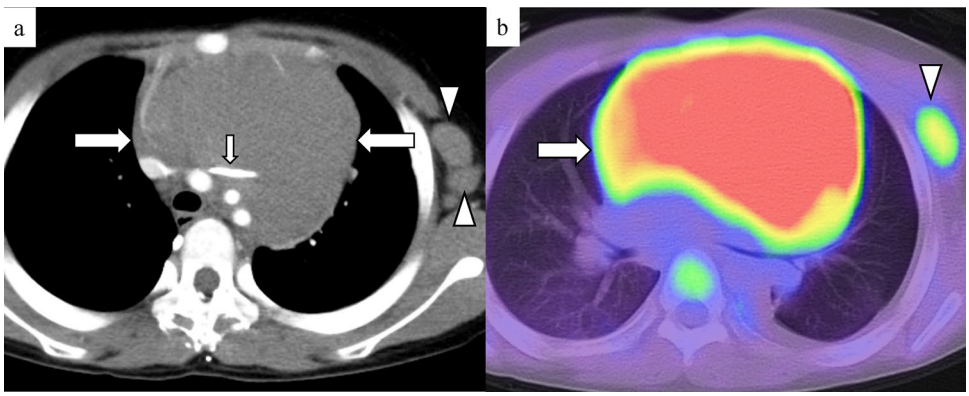

Fig. 7 T-cell lymphoblastic lymphoma in a 9-year-old boy with chest pain and dyspnea. **a** An axial contrast-enhanced CT image (arterial phase) shows a large homogeneous mass (large arrows) in the anterior mediastinum. The aorta, superior vena cava, and trachea are pressed by the mass. The left innominate vein (small arrow) penetrates the mass. Left axillary lymph node enlargements (arrowheads) are also seen. **b** An axial fusion image of the FDG-PET CT image shows high uptake of the mass (arrow; SUVmax: 10.79) and left axillary lymph node enlargement (arrowhead)

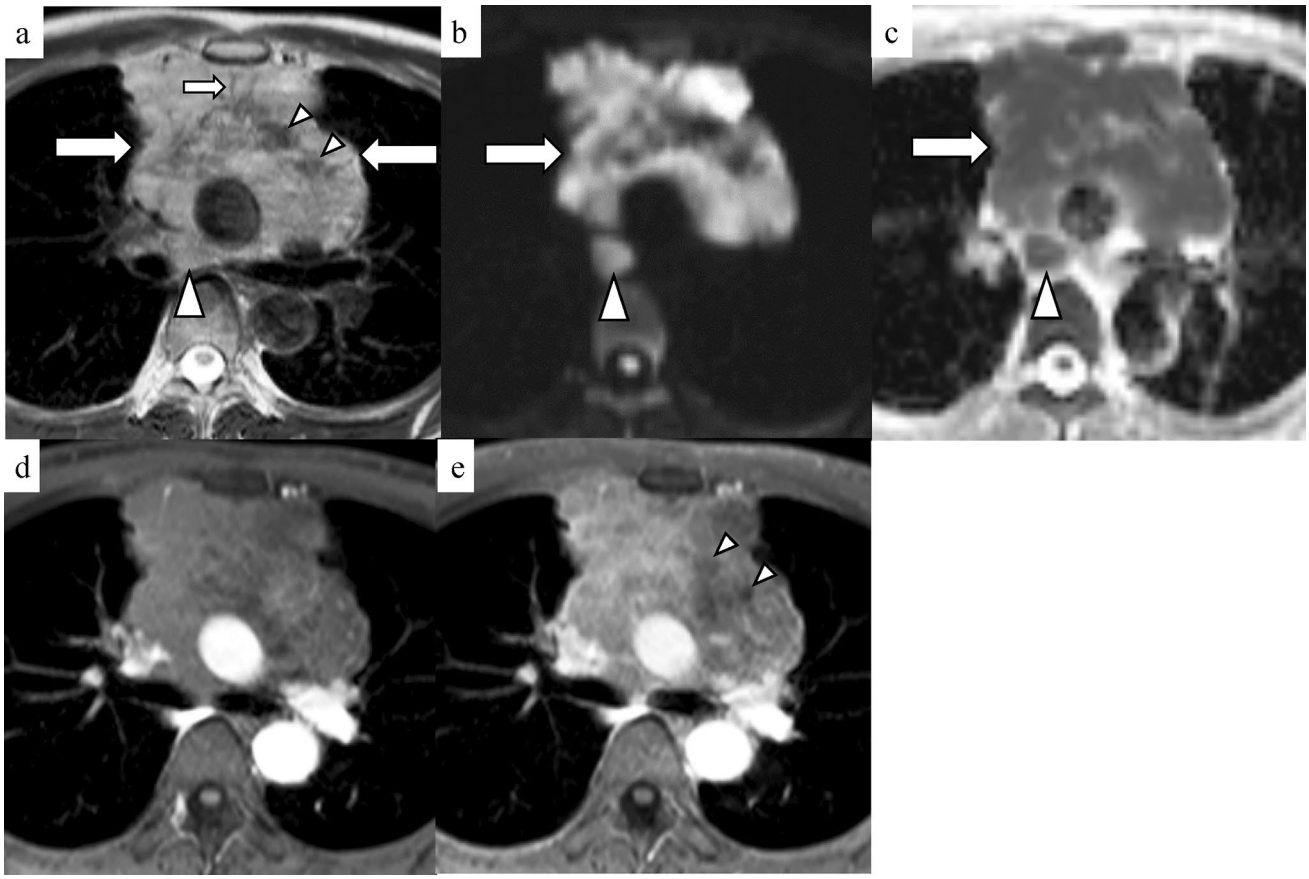

Fig. 8 Seminoma in a 38-year-old man. **a** An axial T2-weighted image shows a heterogeneous mass (large arrows) with an irregular margin in the anterior mediastinum. A peripheral capsule is not seen. Low-signal-intensity septa (small arrow) and low-signal-intensity areas (small arrowheads) which reflect hemorrhagic necrosis are seen in the mass. Mediastinal lymph node enlargement (large arrowhead) adjacent to the mass is also seen. **b** An axial diffusion-weighted image ($b = 1000$ s/mm^2) shows heterogeneous high signal intensity of the mass (arrow) and lymph node enlargement (arrowhead). **c** An axial ADC map shows low ADC values within the mass (arrow; mean ADC value: 0.9×10^{-3} mm^2/s) and lymph node enlargement (arrowhead). **d**, **e** Axial dynamic contrast-enhanced MR images (**d** 60 s; **e** 180 s after the start of injection of the contrast material) show a gradual enhancement of the mass. Small areas without enhancement which reflect necrosis (arrowheads) are seen in the mass

gradual enhancement in the mass (Fig. 8d, e). ADC values of seminoma are low, which may reflect high cellularity in the tumor (Fig. 8c). Nonseminomatous GCTs typically appear more invasive and heterogeneous, reflecting marked necrosis and hemorrhage in the tumor, and lymph node and hematogenous metastases are more common (Fig. 9) compared with pure seminomas [17].

Differential diagnosis of anterior mediastinal solid tumors

Thymic epithelial tumors are usually treated with surgery. In contrast, thoracotomy can be avoided for malignant lymphomas. Malignant GCTs are generally treated with chemotherapy before surgery. Therefore, differential diagnosis of anterior mediastinal solid tumors is important for the choice of treatment strategy. Patients with malignant lymphomas and malignant GCTs are usually younger than patients with thymic epithelial tumors. Tumor markers such as soluble interleukin-2 receptor in malignant lymphomas and α-fetoprotein or human chorionic gonadotropin in nonseminomatous GCTs are useful for the diagnosis. In a study of DWI, ADC values of malignant lymphomas were reported to be lower than those of thymic carcinomas [16]. Yabuuchi et al. reported that malignant lymphomas and GCTs showed larger lesion sizes and higher maximum standardized uptake values (SUVmax) on fluorodeoxyglucose-positron emission tomography (FDG-PET) (Fig. 7b) compared with thymic epithelial tumors [15]. They also reported that the washout enhancement pattern was specific for thymic epithelial tumors (Fig. 2d, e), and all malignant lymphomas (Fig. 6d, e)

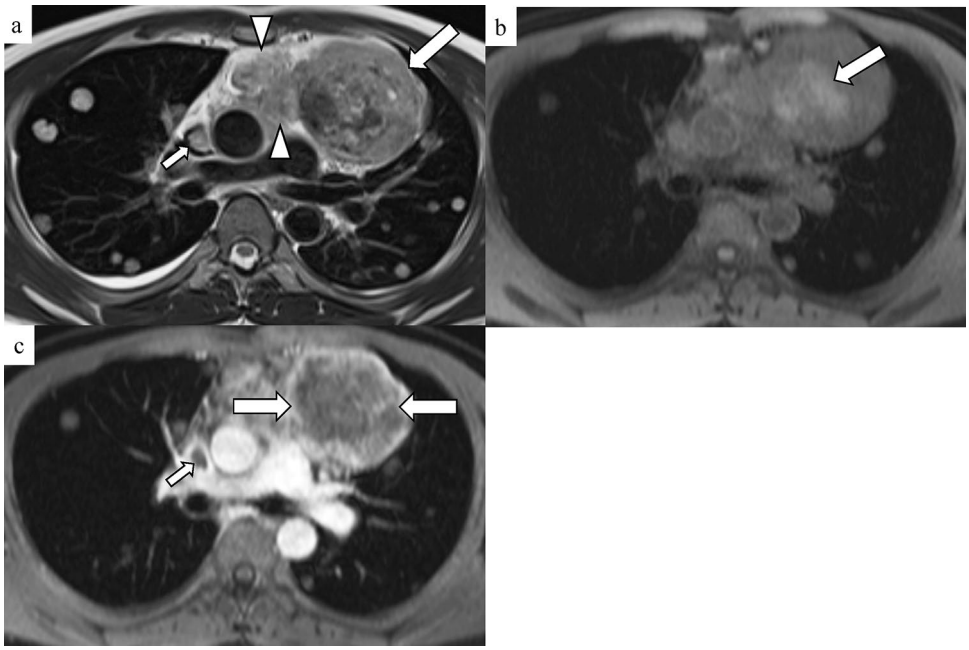

Fig. 9 Embryonal carcinoma in a 32-year-old man. **a** An axial T2-weighted image shows a heterogeneous mass (large arrow) with an irregular margin in the anterior mediastinum. A peripheral capsule is not seen. Mediastinal lymph node metastases (arrowheads), multiple metastases in the bilateral lung, tumor thrombus in the superior vena cava (small arrow), and right pleural effusion are also seen. **b** An axial fat-saturated T1-weighted image shows a high-signal-intensity area (arrow) which reflects hemorrhagic necrosis in the center of the mass. **c** An axial dynamic contrast-enhanced MR image (180 s after the start of injection of the contrast material) shows a large area without enhancement which reflects necrosis (large arrows) and peripheral enhancement of the mass. Tumor thrombus in the superior vena cava (small arrow) is also seen

and GCTs (Fig. 8d, e) showed a gradual or plateau enhancement pattern on dynamic contrast-enhanced MRI [15].

Thymic hyperplasia

Thymic hyperplasia is classified histologically into true hyperplasia and lymphoid hyperplasia. True thymic hyperplasia is an increase in the size of the thymus with normal gross and histological appearance and commonly occurs as rebound thymic hyperplasia secondary to atrophy caused by chemotherapy for malignancy [13]. Thymic lymphoid hyperplasia is pathologically diagnosed by the presence of hyperplastic lymphoid germinal centers in the medulla of the thymus, in association with a lymphocytic and plasma cell infiltrate [13]. Thymic lymphoid hyperplasia is commonly associated with autoimmune diseases such as MG. Thymic hyperplasia appears as a round or box-shaped mass in children and a flat triangular mass in adults in the anterior mediastinum (Fig. 10) [13]. Chemical shift MRI is reported to be useful to detect fat tissues intervening between thymic tissues in thymic hyperplasia (Fig. 10) and to differentiate thymic hyperplasia from thymic epithelial tumors [18]. It is important to differentiate rebound thymic hyperplasia from recurrence in patients after chemotherapy for malignancies.

Thymolipoma

Thymolipoma is a rare benign tumor that contains fat and non-neoplastic thymic tissues. The average age of patients is 22–26 years, with no gender predominance, and most patients are asymptomatic [19]. Thymolipomas typically show a large, well-defined, and soft mass in the anterior mediastinum and pericardial region and may mimic cardiomegaly on chest radiograph. CT and MRI show a mass comprised of intermingled soft tissue and fat tissue in the anterior mediastinum (Fig. 11) [19]. Differential diagnosis of thymolipoma includes lipoma and liposarcoma.

Intrathoracic goiter

The majority of intrathoracic goiters are substernal extensions of cervical goiters. They commonly occur in the superior portion of the mediastinum and may extend to the anterior and middle mediastinum [20]. Approximately 2% of cases show no evident connection to the cervical thyroid gland and are thought to arise from an ectopic thyroid gland in the mediastinum (Fig. 12) [21]. It might be difficult to differentiate preoperatively intrathoracic goiters arisen from an ectopic thyroid from other anterior mediastinal solid tumors

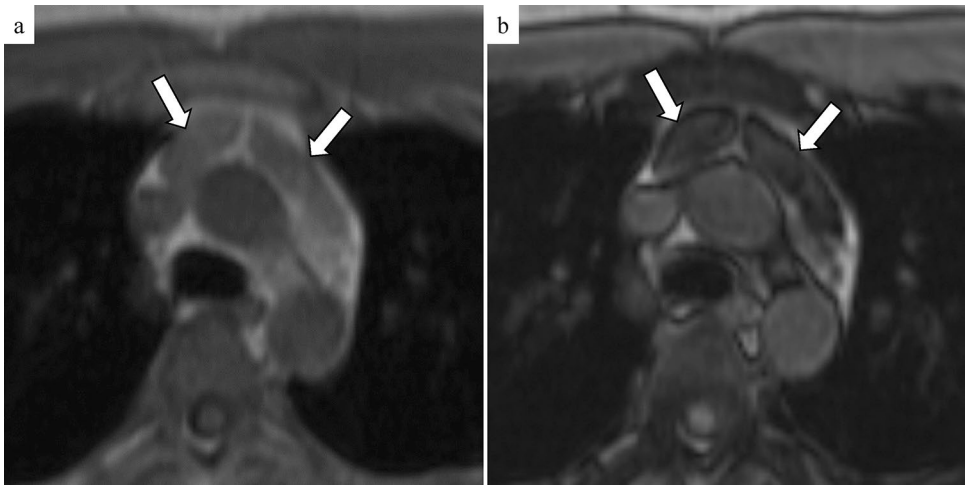

Fig. 10 Thymic hyperplasia in a 26-year-old man with hyperthyroidism. **a**, **b** Axial in-phase (**a**) and opposed-phase (**b**) T1-weighted images show a flat triangular lesion (arrows) in the anterior mediastinum. The opposed-phase image shows decreasing signal intensity within the lesion (arrows) compared with the in-phase image, which reflect intermingled fat tissues in thymic hyperplasia

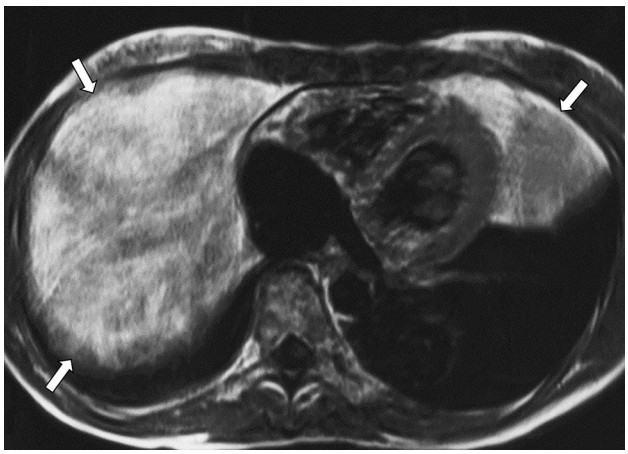

Fig. 11 Thymolipoma in a 15-year-old woman. An axial T1-weighted image shows a large well-circumscribed mass (arrows) in the pericardial region. The mass appears to intermingle areas of high signal intensity reflecting fat and areas of intermediate signal intensity reflecting thymic and fibrous tissues in the lesion

such as thymic epithelial tumors. Adenomatous goiter is the most common histologically, and carcinomas occur in 2–38% of intrathoracic goiters [20, 21]. Thyroid tissues may show high attenuation due to intrinsic iodine on plain CT [20]. Adenomatous goiters show multiple nodules, and calcifications, cystic change (Fig. 12), and hemorrhage in the lesion are common [20]. Dynamic contrast-enhanced CT and MRI show rapid and marked enhancement in the early phase (Fig. 12) and washout of contrast media in the delayed phase, which reflect hypervascularity of adenomatous goiter. Although differentiation between benign goiters and thyroid carcinomas is difficult, invasion to the surrounding structures and lymph node enlargement should be considered suspicious for thyroid carcinomas. ^{123}I-scintigraphy is useful for diagnosis of ectopic intrathoracic goiters [20].

Fig. 12 Ectopic intrathoracic goiter in a 62-year-old woman. A coronal contrast-enhanced CT image shows a well-circumscribed nodule with peripheral nodular marked enhancements (arrows) in the superior portion of the mediastinum. There is no connection between the nodule and thyroid gland (arrowheads)

Ectopic parathyroid adenoma

Ectopic mediastinal parathyroid adenomas occur in 22% of patients with hyperparathyroidism [22]. They usually arise from inferior parathyroid glands and occur in the superior portion of the mediastinum and anterior mediastinum, usually near or within the thymus due to a common embryologic origin from the third and fourth brachial pouches [23]. Ectopic parathyroid adenomas show a small solid nodule with rapid and marked enhancement on contrast-enhanced CT (Fig. 13) and MRI. Calcification, cystic change, and

hemorrhage within the lesion may be seen [20]. ^{99m}Tc-methoxy-isobutyl-isonitrile (MIBI) scintigraphy has high sensitivity for detection of parathyroid adenomas [24].

Neurogenic tumors

Most mediastinal neurogenic tumors arise in the posterior mediastinum, but some may occur from nerves in other locations. The phrenic nerves pass between the subclavian arteries and veins, then enter the thorax and cross the root of the lung anteriorly, and finally pass over the heart between the pericardium and mediastinal pleura [1]. The vagus nerves pass between the subclavian artery and vein, enter the thorax and descend along the esophagus in the mediastinum [1]. The right recurrent laryngeal nerve arises from the right vagus nerve, hooks around the right subclavian artery, and ascends between the trachea and esophagus. The left vagus nerve descends on the lateral side of the aortic arch and gives rise to the left recurrent laryngeal nerve, which hooks around the aortic arch and ascends between the trachea and esophagus [1]. Peripheral nerve tumors such as schwannoma arising from vagus (Fig. 14) and phrenic nerves may occur in the superior portion of the mediastinum and anterior mediastinum [25].

Benign peripheral nerve tumors typically show a well-circumscribed solid mass with a thin fibrous capsule. Cystic change and hemorrhage are common in schwannomas. The Antoni A area of schwannomas is composed of cellular spindle cells and displays relatively low signal intensity on T2-weighted images and relatively strong contrast enhancement [26]. The Antoni B area is hypocellular and contains myxomatous loosely arranged tissue, with very high signal intensity on T2-weighted images and gradual and weak contrast enhancement. Neurofibromas typically show gradual and weak contrast enhancement, which reflects myxomatous and fibrous tissues in the tumor [26]. Malignant peripheral nerve sheath tumors (MPNSTs) are rare spindle cell sarcomas arising from a peripheral nerve or neurofibroma or showing nerve tissue differentiation [27]. MPNSTs are associated with neurofibromatosis type 1 in 25–70% of cases, and a sudden increase in the size of a previously stable neurofibroma together with emergence of neurologic symptoms suggests malignant transformation to MPNST [27]. MPNSTs commonly involve major nerve trunks, such as the sciatic nerve and brachial plexus [27], but rarely occur in the intrathoracic phrenic and vagus nerves [28, 29]. MPNSTs typically show a heterogeneous mass with peripheral enhancement due to central necrosis on contrast-enhanced CT and MRI [26, 27]. The "target sign" on T2-weighted images, comprising a peripheral high-signal-intensity area and central low-signal-intensity area, is common in schwannomas and neurofibromas, but rare in MPNSTs [30].

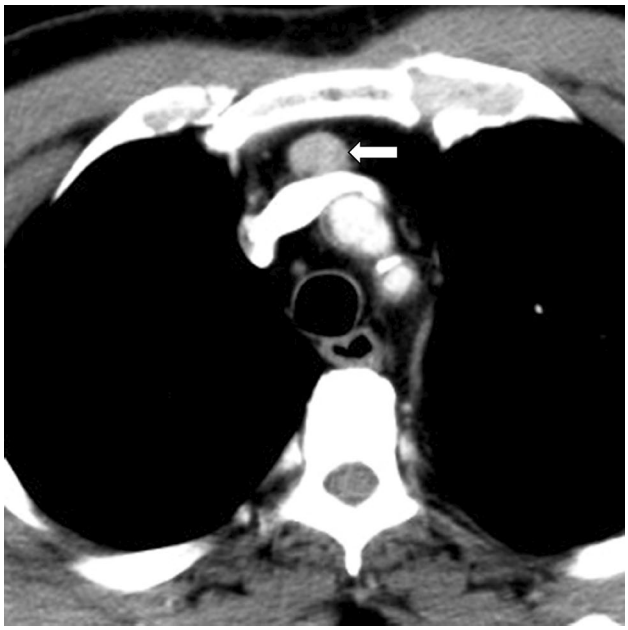

Fig. 13 Ectopic parathyroid adenoma in a 60-year-old man. An axial contrast-enhanced CT image shows a well-circumscribed nodule (arrow) with a marked enhancement in the superior portion of the mediastinum

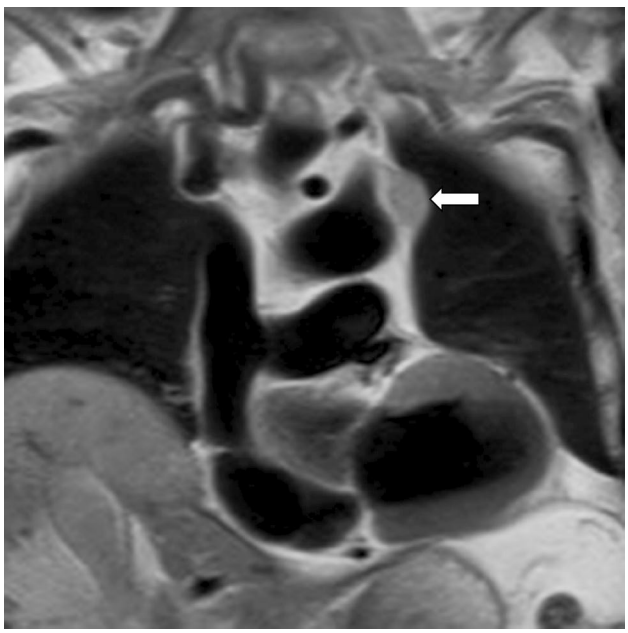

Fig. 14 Schwannoma arising from the left vagus nerve in a 77-year-old man who had hoarseness. A coronal T2-weighted image shows a well-circumscribed nodule with a teardrop shape (arrow) in the left lateral side of the aortic arch

The mediastinal paraganglia are predominantly concentrated in two locations. The paraganglia found along the sympathetic chain of the paravertebral region are known as the aortosympathetic paraganglia, and those located along the great vessels are known as the aortopulmonary paraganglia, or sometimes the aortic body [31]. The aortopulmonary paraganglia are characteristically found in one of five locations within the thorax: between the ascending aorta and pulmonary trunk, either anteriorly or posteriorly, adjacent to the aortic root (the coronary paraganglia); associated with the groove between the ductus arteriosus and the pulmonary artery (the pulmonary paraganglia); between the right subclavian and right common carotid arteries; between the left subclavian and left common carotid arteries; or caudal to the left subclavian artery adjacent to the aortic arch [31]. Aortopulmonary paragangliomas occur in the superior portion of the mediastinum, anterior mediastinum (Fig. 15) and middle mediastinum [25]. Paragangliomas appear as a well- or ill-defined mass and may be heterogeneous because of hemorrhage or necrosis in the lesion (Fig. 15) [26]. Paraganglioma are hypervascular and show rapid intense enhancement on contrast-enhanced CT and MRI. Feeding vessels (Fig. 15) and flow voids may be seen within or around the lesion [26]. A "salt and pepper" appearance, adjacent high-signal-intensity regions which reflect slow flow within the tumor vessels or hemorrhage and low-signal-intensity regions which reflect high flow within tumor vessels on T2-weighted images, may be seen in paragangliomas [32].

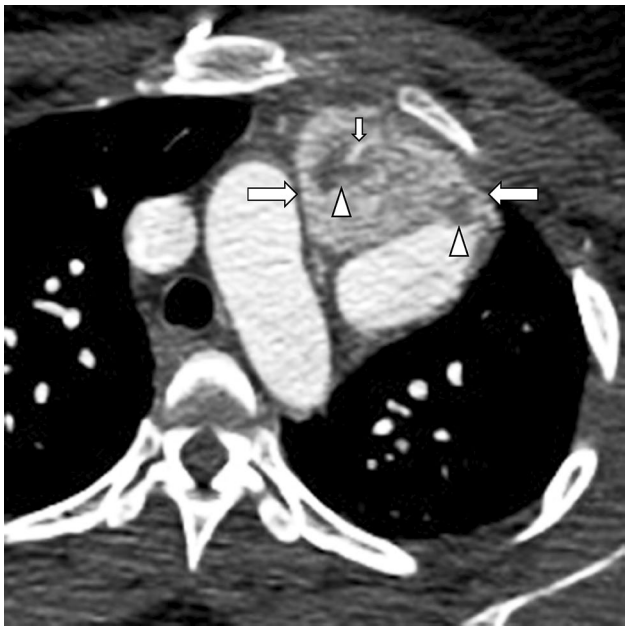

Fig. 15 Paraganglioma arising from an aortopulmonary paraganglion in a 25-year-old woman. An axial contrast-enhanced CT image (arterial phase) shows a heterogeneous mass with an irregular margin (large arrows) between the aortic arch and main trunk of the pulmonary artery. Low attenuation areas which reflect necrosis (arrowheads) and a feeding vessel (small arrow) are seen in the mass

Imaging features of anterior mediastinal cystic lesions

Thymic cysts and pericardial cysts are common cystic lesions in the anterior mediastinum. Mature cystic teratomas are the most common mediastinal GCTs and usually occur in the anterior mediastinum. Cystic change is common in intrathoracic goiter. Ectopic parathyroid cysts may occur in the superior portion of the mediastinum and anterior mediastinum. Marked cystic change in neurogenic tumors may occur and may resemble a cystic lesion. Mediastinal lymphangiomas are rare, but the reported cases commonly occur in the anterior mediastinum and superior portion of the mediastinum.

On imaging findings of mediastinal cystic lesions, unilocularity vs. multilocularity, cyst wall thickness, cystic fluid (serous, viscous, or hemorrhagic), and calcification, fat, and solid components in the cyst should be evaluated. Cystic lesions containing solid components may include malignancy. Cystic lesions containing viscous or hemorrhagic fluid may show high attenuation and mimic a solid lesion on plain CT. MRI is useful for differentiation between mediastinal cystic and solid lesions without contrast media [33, 34]. MRI is superior to CT for the detection of small amounts of fat or hemorrhage. The signal intensity on DWI and the ADC values vary according to the type of fluid in the cyst. Viscous or hemorrhagic fluid may show high signal intensity on DWI and relatively low ADC values compared with serous fluid. DWI may be useful to detect malignant solid components in the cystic lesion without contrast media.

Thymic cysts

Thymic cysts are divided into congenital cysts or acquired cysts. Congenital thymic cysts are derived from a remnant of the thymopharyngeal duct and are usually small unilocular cysts containing serous or hemorrhagic fluid [20]. Acquired thymic cysts are usually multilocular. Such cysts are called multilocular thymic cysts (MLTCs); they have relatively thick walls and contain serous, viscous, or hemorrhagic (motor-oil-like) fluid [20]. MLTCs are associated with Sjögren's syndrome (Fig. 16) and human immunodeficiency virus infection [20, 35]. Viscous or hemorrhagic fluid in the cyst shows relatively high signal intensity on T1-weighted images (Fig. 16b) [35, 36]. Viscous fluid may show slightly high signal intensity on DWIs and relatively low ADC values compared with serous fluid. MLTCs are reported to be associated with thymomas (Fig. 17), thymic

carcinomas, and seminomas, which occur as solid components within MLTCs [37, 38].

Mucosa-associated lymphoid tissue lymphoma

Mucosa-associated lymphoid tissue (MALT) lymphomas are low-grade B cell lymphomas and rarely occur in the thymus. Thymic MALT lymphomas are reported to show a multilocular cyst that mimics MLTC [39]. Cases with a solid mass or a mixture of solid and cystic components are also reported. The cysts in thymic MALT lymphoma may show various signal intensity on T1-weighted and T2-weighted images according to serous, viscous, or hemorrhagic fluid [39].

Pericardial cyst

Pericardial or mesothelial cysts result from aberrations in the formation of coelomic (somatic) cavities and are uncommon benign congenital anomalies [36]. These cysts are common in the anterior cardiophrenic angle, more frequently on the right side [36]. They typically appear as a well-defined, round or oval unilocular cyst with a thin wall [36]. The cyst fluid is usually serous and could be hemorrhagic. Mural calcification is rare. Cysts connected to the pericardial space are called pericardial diverticula and are common in the right paratracheal region.

Cystic teratoma

Mature cystic teratomas are the most common GCT and usually occur in the anterior mediastinum. They typically appear as unilocular or multilocular cysts with relatively thick walls, and contain fat, calcifications, hair balls, and in rare cases, teeth [40]. In 15% of mediastinal teratomas, fat tissues and calcifications are not detected on CT (Fig. 18a) [40]. Chemical shift MRI can detect tiny fat tissues within the lesions (Fig. 18b, c). Cystic teratomas usually contain viscous fluid with keratinization tissues which may show high signal intensity on DWI (Fig. 18d) and relatively low ADC values (Fig. 18e) compared with a serous cyst. 36% of

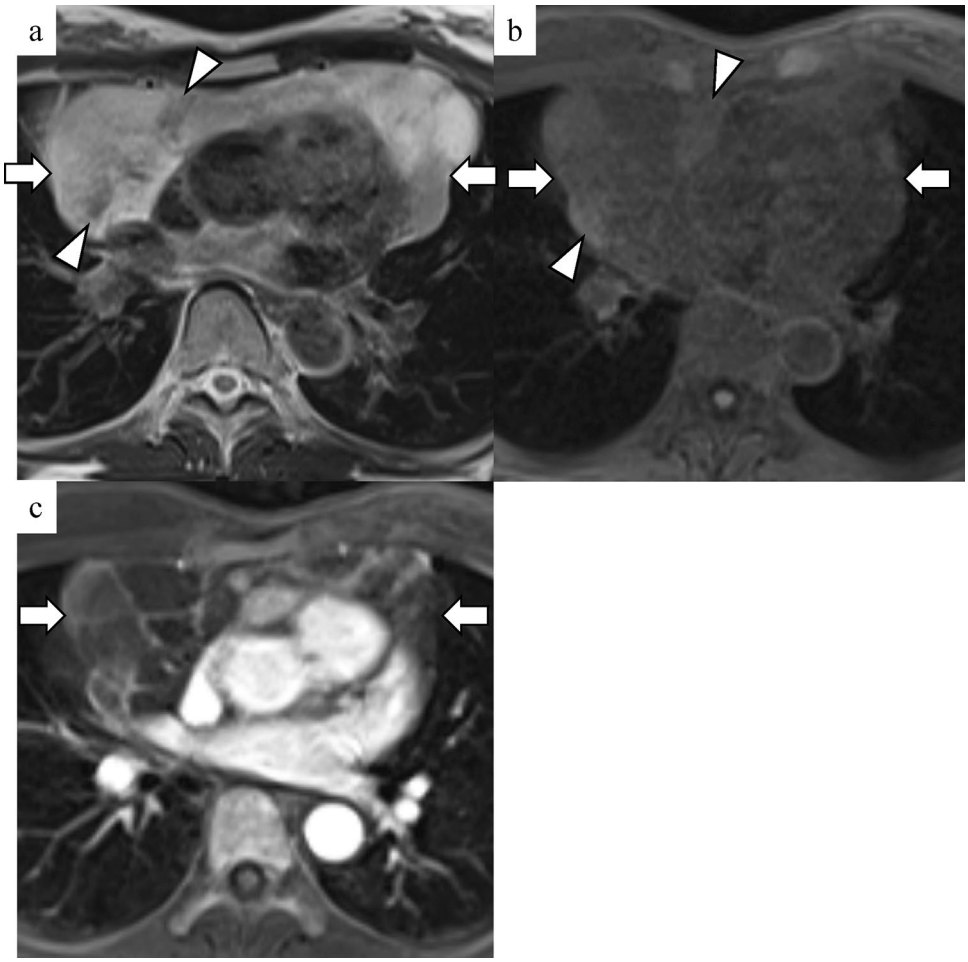

Fig. 16 Multilocular thymic cyst in a 43-year-old woman with Sjögren's syndrome. a, b) Axial T2-weighted image (**a**) and axial fat-saturated T1-weighted image (**b**) show a large multilocular cyst (arrows) in the anterior mediastinum. Slightly low-signal-intensity areas (arrowheads) on the T2-weighted image and slightly high-signal-intensity areas (arrowheads) on the fat-saturated T1-weighted image reflect viscous fluid in the cyst. **c** An axial dynamic contrast-enhanced MR image (180 s after the start of injection of the contrast material) shows enhancements of the wall and septa of the cyst (arrows)

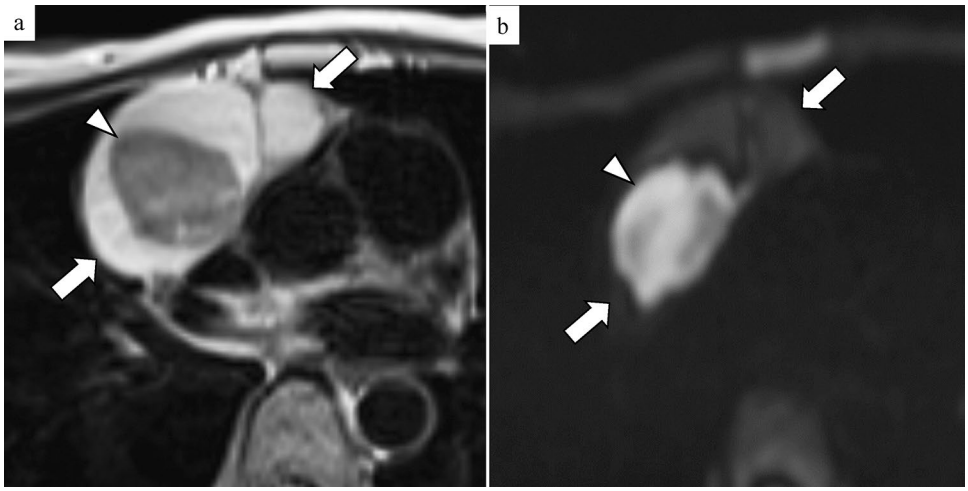

Fig. 17 **a** Type B2 thymoma associated with multilocular thymic cyst in a 42-year-old woman. **b** An axial T2-weighted image shows a multilocular cyst (arrows) with a solid component (arrowhead) in the anterior mediastinum. **c** An axial diffusion-weighted image shows high signal intensity of the solid component (arrowhead) in the cyst (arrows)

mediastinal teratomas are reported to rupture to the mediastinum, lung (Fig. 19), or pleural cavity [41]. Patients with ruptured mediastinal teratomas have symptoms such as cough, chest pain, fever, or trichoptysis [41]. Ruptured teratomas may show an irregular, ill-defined, invasive, or heterogeneous mass with lymph node enlargements (Fig. 19), which mimic malignancy [41].

Mediastinal immature teratomas are very rare (1% of mediastinal teratomas) and have male predominance [42]. Reported cases of mediastinal immature teratomas show

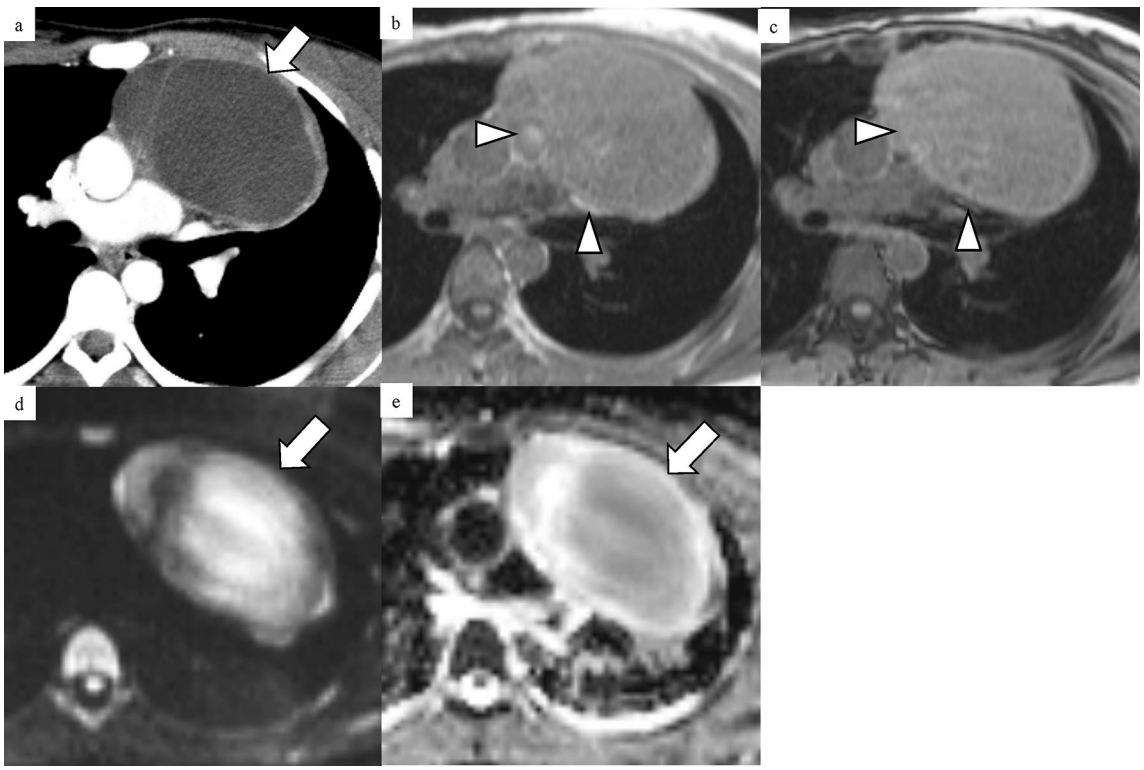

Fig. 18 Mature cystic teratoma in a 26-year-old woman. **a** An axial contrast-enhanced CT image shows a multilocular cyst with a thick wall (arrow). Neither fat nor calcification is seen in the cyst. **b**, **c** An axial in-phase T1-weighted image (**b**) shows slightly high-signal-intensity areas (arrowheads) in the cyst, and an axial opposed-phase T1-weighted image (**c**) shows decreasing signal intensity of these areas (arrowheads), reflecting fat tissues. **c** An axial diffusion-weighted image ($b = 1000$ s/mm^2) shows high signal intensity that reflects viscous fluid in the cyst (arrow). **d** An axial ADC map shows relatively low ADC values (mean ADC value: 1.4×10^{-3} mm^2/s) of the fluid in the cyst (arrow)

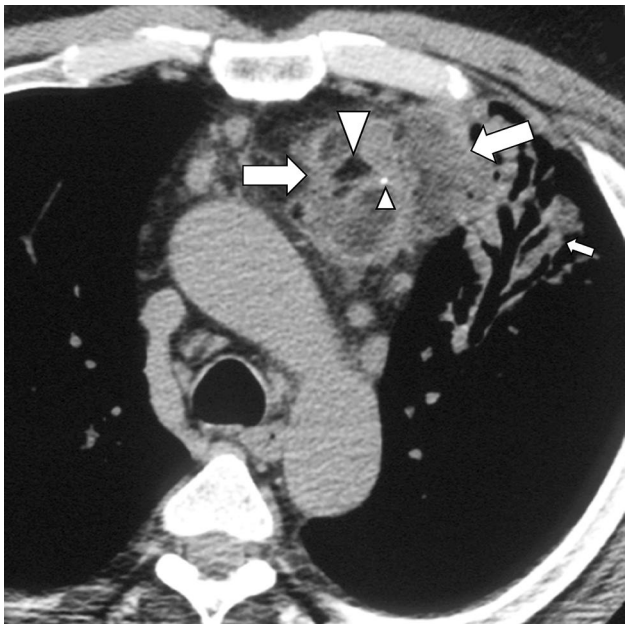

Fig. 19 Ruptured mature cystic teratoma in a 44-year-old man who had chest pain, cough and sputum. An axial plain CT image shows a multilocular cyst (large arrows) with a thick wall and septa in the anterior mediastinum. A calcification (small arrowhead) and fat (large arrowhead) are seen in the cyst. Mediastinal lymph node enlargements and consolidation in the left lung (small arrow) are also seen. Rupture of the mediastinal mature cystic teratoma to the left lung was confirmed by the surgery

Fig. 20 Ectopic parathyroid cyst in a 56-year-old man. An axial contrast-enhanced CT image shows a unilocular cyst with a thin wall (arrows) in the superior portion of the mediastinum. Serous cyst fluid and parathyroid tissues in the cyst wall were confirmed on the pathological findings

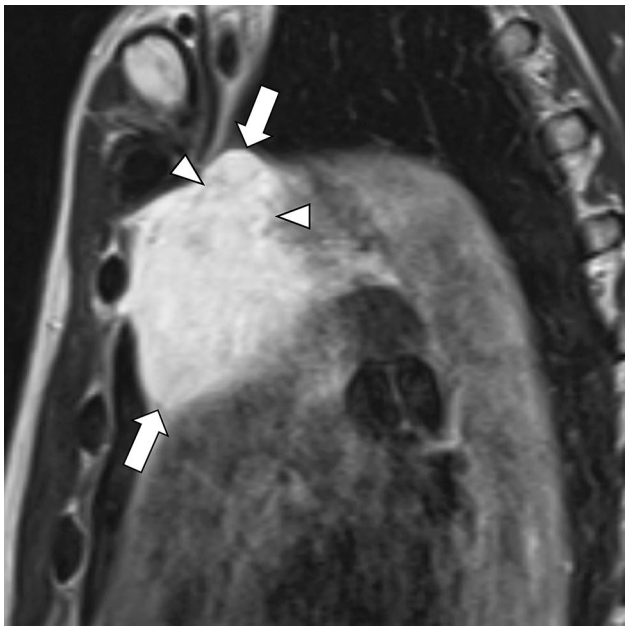

Fig. 21 Cystic lymphangioma in a 56-year-old man. A sagittal T2-weighted image shows a multilocular cyst (arrows) with a thin wall and septa (arrowheads) in the anterior mediastinum

large and heterogeneous solid components and scattered small fat tissues and calcifications in the lesions [42]. GCTs with somatic-type malignancy are known as teratomas with malignant transformation and account for 2% of GCTs in males [6]. Among GCTs with somatic-type malignancy 25–30% occur in the mediastinum [6]. Sarcomas (rabdomyosarcomas are the most common) account for 63%, and carcinomas (intestinal type adenocarcinomas are the most common) account for the other 37% of the somatic-type malignancies associated with GCTs [6]. The reported cases show large invasive solid components in mature cystic teratomas [43].

Thyroid cyst and parathyroid cyst

Cystic change is common in intrathoracic goiter, but ectopic mediastinal thyroid cyst is very rare. Mediastinal parathyroid cyst is also rare, and the median age of the reported cases is 55 year with no gender predominance [44]. These cysts are common in the superior portion of the mediastinum and anterior mediastinum, and non-functional lesions are common than functioning lesions [44]. Mediastinal parathyroid cysts show a small thin-walled unilocular cyst containing serous fluid (Fig. 20) [45].

Cystic lymphangioma

Lymphangiomas are rare, benign congenital malformations consisting of focal proliferations of well-differentiated lymphatic tissue that are present in a multicystic or sponge-like accumulation [36]. The majority of lymphangiomas are discovered during the first 2 years of life. They are most common in the neck and axilla, and about 10% extend into the mediastinum [36]. Approximately 1% of all lymphangiomas are confined to the chest, and lymphangiomas represent 0.7–4.5% of all mediastinal tumors [36]. Lymphangiomas are common in the anterior mediastinum and superior portion of the mediastinum. They are classified histologically as capillary, cavernous, or cystic (hygroma), depending on the size of the lymphatic channels they contain [36]. Cystic type is the most common in the mediastinum. Although patients with mediastinal lymphangioma are usually asymptomatic, compression of the mediastinal structures can result in chest pain, cough, and dyspnea. Complications of mediastinal lymphangioma include infection, airway compromise, chylothorax, and chylopericardium [36]. Cystic lymphangiomas typically show a well-circumscribed multilocular cyst with a thin wall and septa (Fig. 21). The cyst fluid is chylous and rarely hemorrhagic. Stippled or curvilinear calcifications are rarely seen in the cyst wall or septa [46].

Conclusion

Anterior mediastinal lesions include various solid and cystic tumors. Location and imaging features are important for the diagnosis of the mediastinal lesions. CT-based mediastinal compartment classification is useful for accurate evaluation of location of mediastinal lesions. CT and MRI findings reflect pathological features of mediastinal lesions. MRI can provide additional information of imaging features of mediastinal solid and cystic lesions. Integrated knowledge of the pathological and imaging features of mediastinal lesions and clinical information of the patient are important for an accurate diagnosis.

Funding The authors declare they have no funding.

Compliance with ethical standards

Conflict of interest The authors declare that they have no conflict of interest.

Human and animal rights statement This article does not contain any studies with human participants or animals performed by any of the authors.

References

1. Shah P. Chapter 59, Mediastinum. In: Standring S, editor. Gray's anatomy: the anatomical basis of clinical practice. 39th ed. Philadelphia: Elsevier; 2005. p. 977–994.
2. Felson B. Chapter 11, The mediastinum. Chest roentgenology. Philadelphia: WB Saunders; 1973. p. 389–420.
3. Fujimoto K, Hara M, Tomiyama N, Kusumoto M, Sakai F, Fujii Y. Proposal for a new mediastinal compartment classification of transverse plane images according to the Japanese Association for Research on the Thymus (JART) General Rules for the Study of Mediastinal Tumors. Oncol Rep. 2014;31:565–72.
4. Carter BW, Tomiyama N, Bhora FY, Rosado de Christenson ML, Nakajima J, Boiselle PM, et al. A modern definition of mediastinal compartments. J Thorac Oncol. 2014;9:S97–101.
5. Razek AA, Elmorsy A, Elshafey M, Elhadedy T, Hamza O. Assessment of mediastinal tumors with diffusion-weighted single-shot echo-planar MRI. J Magn Reson Imaging. 2009;30:535–40.
6. Travis WD, Brambilla E, Burke AP, Marx A, Nicholson AG. Chapter 3, Tumours of the thymus. WHO Classification of Tumours of the Lung, Pleura, Thymus and Heart. 4th ed. Lyon: International Agency for Research on Cancer (IARC); 2015. p. 183–298.
7. Sadohara J, Fujimoto K, Muller NL, Kato S, Takamori S, Ohkuma K, et al. Thymic epithelial tumors: comparison of CT and MR imaging findings of low-risk thymomas, high-risk thymomas, and thymic carcinomas. Eur J Radiol. 2006;60:70–9.
8. Tomiyama N, Johkoh T, Mihara N, Honda O, Kozuka T, Koyama M, et al. Using the World Health Organization Classification of thymic epithelial neoplasms to describe CT findings. AJR Am J Roentgenol. 2002;179:881–6.
9. Sakai S, Murayama S, Soeda H, Matsuo Y, Ono M, Masuda K. Differential diagnosis between thymoma and non-thymoma by dynamic MR imaging. Acta Radiol. 2002;43:262–8.
10. Abdel Razek AA, Khairy M, Nada N. Diffusion-weighted MR imaging in thymic epithelial tumors: correlation with World Health Organization classification and clinical staging. Radiology. 2014;273:268–75.
11. Priola AM, Priola SM, Giraudo MT, Gned D, Fornari A, Ferrero B, et al. Diffusion-weighted magnetic resonance imaging of thymoma: ability of the Apparent Diffusion Coefficient in predicting the World Health Organization (WHO) classification and the Masaoka-Koga staging system and its prognostic significance on disease-free survival. Eur Radiol. 2016;26:2126–38.
12. Shimamoto A, Ashizawa K, Kido Y, Hayashi H, Nagayasu T, Kawakami A, et al. CT and MRI findings of thymic carcinoid. Br J Radiol. 2017;90:20150341. https://doi.org/10.1259/bjr.20150341.
13. Takahashi K, Al-Janabi NJ. Computed tomography and magnetic resonance imaging of mediastinal tumors. J Magn Reson Imaging. 2010;32:1325–39.
14. Tateishi U, Muller NL, Johkoh T, Onishi Y, Arai Y, Satake M, et al. Primary mediastinal lymphoma: characteristic features of the various histological subtypes on CT. J Comput Assist Tomogr. 2004;28:782–9.
15. Yabuuchi H, Matsuo Y, Abe K, Baba S, Sunami S, Kamitani T, et al. Anterior mediastinal solid tumours in adults: characterisation using dynamic contrast-enhanced MRI, diffusion-weighted MRI, and FDG-PET/CT. Clin Radiol. 2015;70:1289–98.
16. Zhang W, Zhou Y, Xu XQ, Kong LY, Xu H, Yu TF, et al. A Whole-tumor histogram analysis of apparent diffusion coefficient maps for differentiating thymic carcinoma from lymphoma. Korean J Radiol. 2018;19:358–65.
17. Tian L, Liu LZ, Cui CY, Zhang WD, Kuang YL. CT findings of primary non-teratomatous germ cell tumors of the mediastinum—a report of 15 cases. Eur J Radiol. 2012;81:1057–61.

18. Inaoka T, Takahashi K, Mineta M, Yamada T, Shuke N, Okizaki A, et al. Thymic hyperplasia and thymus gland tumors: differentiation with chemical shift MR imaging. Radiology. 2007;243:869–76.
19. Rosado-de-Christenson ML, Pugatch RD, Moran CA, Galobardes J. Thymolipoma: analysis of 27 cases. Radiology. 1994;193:121–6.
20. Strollo DC, Rosado de Christenson ML, Jett JR. Primary mediastinal tumors. Part 1: tumors of the anterior mediastinum. Chest. 1997;112:511–22.
21. Maeda A, Shimizu K, Yukawa T, Hirami Y, Nakata M. A case of aberrant mediastinal goiter. Jpn J Assoc Chest Surg. 2010;24:195–9 **(Japanese)**.
22. Clark OH. Mediastinal parathyroid tumors. Arch Surg. 1988;123:1096–100.
23. Nathaniels EK, Nathaniels AM, Wang CA. Mediastinal parathyroid tumors: a clinical and pathological study of 84 cases. Ann Surg. 1970;171:165–70.
24. Gotthardt M, Lohmann B, Behr TM, Bauhofer A, Franzius C, Schipper ML, et al. Clinical value of parathyroid scintigraphy with technetium-99m methoxyisobutylisonitrile: discrepancies in clinical data and a systematic metaanalysis of the literature. World J Surg. 2004;28:100–7.
25. Nakazono T, Yamaguchi K, Egashira R, Takase Y, Nojiri J, Mizuguchi M, et al. CT-based mediastinal compartment classifications and differential diagnosis of mediastinal tumors. Jpn J Radiol. 2019;37:117–34.
26. Nakazono T, White CS, Yamasaki F, Yamaguchi K, Egashira R, Irie H, et al. MRI findings of mediastinal neurogenic tumors. AJR Am J Roentgenol. 2011;197:W643–W652652.
27. Murphey MD, Smith WS, Smith SE, Kransdorf MJ, Temple HT. From the archives of the AFIP. Imaging of musculoskeletal neurogenic tumors: radiologic-pathologic correlation. Radiographics. 1999;19:1253–80.
28. Jakobsen EB, Pettersson G, Pedersen H, Nielsen HW. Neurofibrosarcoma of the intrathoracic vagus nerve Case report. Scand J Thorac Cardiovasc Surg. 1993;27:109–11.
29. Koezuka S, Hata Y, Sato F, Otsuka H, Makino T, Tochigi N, et al. Malignant peripheral nerve sheath tumor in the anterior mediastinum: a case report. Mol Clin Oncol. 2014;2:987–90.
30. Bhargava R, Parham DM, Lasater OE, Chari RS, Chen G, Fletcher BD. MR imaging differentiation of benign and malignant peripheral nerve sheath tumors: use of the target sign. Pediatr Radiol. 1997;27:124–9.
31. Balcombe J, Torigian DA, Kim W, Miller WT Jr. Cross-sectional imaging of paragangliomas of the aortic body and other thoracic branchiomeric paraganglia. Am J Roentgenol. 2007;188:1054–8.
32. Olsen WL, Dillon WP, Kelly WM, Norman D, Brant-Zawadzki M, Newton TH. MR imaging of paragangliomas. Am J Roentgenol. 1987;148:201–4.
33. Shin KE, Yi CA, Kim TS, Lee HY, Choi YS, Kim HK, et al. Diffusion-weighted MRI for distinguishing non-neoplastic cysts from solid masses in the mediastinum: problem-solving in mediastinal masses of indeterminate internal characteristics on CT. Eur Radiol. 2014;24:677–84.
34. Tomiyama N, Honda O, Tsubamoto M, Inoue A, Sumikawa H, Kuriyama K, et al. Anterior mediastinal tumors: diagnostic accuracy of CT and MRI. Eur J Radiol. 2009;69:280–8.
35. Leonidas JC, Berdon WE, Valderrama E, Neveling U, Schuval S, Weiss SJ, et al. Human immunodeficiency virus infection and multilocular thymic cysts. Radiology. 1996;198:377–9.
36. Jeung MY, Gasser B, Gangi A, Bogorin A, Charneau D, Wihlm JM, et al. Imaging of cystic masses of the mediastinum. Radiographics. 2002;22:S79–93.
37. Inui M, Nitadori JI, Tajima S, Yoshioka T, Hiyama N, Watadani T, et al. Mediastinal seminoma associated with multilocular thymic cyst. Surg Case Rep. 2017;3:7. https://doi.org/10.1186/s40792-016-0278-7.
38. Shen X, Jin Y, Shen L, Sun Y, Chen H, Li Y. Thymoma and thymic carcinoma associated with multilocular thymic cyst: a clinicopathologic analysis of 18 cases. Diagn Pathol. 2018;13:41. https://doi.org/10.1186/s13000-018-0719-7.
39. Kuroki S, Nasu K, Murakami K, Hayashi T, Sekiguchi R, Nishida H, et al. Thymic MALT lymphoma: MR imaging findings and their correlation with histopathological findings on four cases. Clin Imaging. 2004;28:274–7.
40. Moeller KH, Rosado-de-Christenson ML, Templeton PA. Mediastinal mature teratoma: imaging features. Am J Roentgenol. 1997;169:985–90.
41. Sasaka K, Kurihara Y, Nakajima Y, Seto Y, Endo I, Ishikawa T, et al. Spontaneous rupture: a complication of benign mature teratomas of the mediastinum. Am J Roentgenol. 1998;170:323–8.
42. Carter D, Bibro MC, Touloukian RJ. Benign clinical behavior of immature mediastinal teratoma in infancy and childhood: report of two cases and review of the literature. Cancer. 1982;49:398–402.
43. Takahashi M, Okumura N, Matsuoka T, Yamashina A, Nakano J, Kameyama K. Teratoma with naturally occurring malignant transformation in a child. Ann Thorac Cardiovasc Surg. 2011;17:588–90.
44. Kobayashi S, Karube Y, Araki O, Chida M, Miyoshi S. A case of mediastinal parathyroid cyst: review of 133 cases of mediastinal parathyroid cyst in the literature. J Jpn Assoc Chest Surgery. 2010;24:1041–5 **(Japanese)**.
45. Kato H, Kanematsu M, Kiryu T, Iwata H, Shirahashi K, Matsumoto S, et al. Nonfunctional mediastinal parathyroid cyst: imaging findings in two cases. Clin Imaging. 2008;32:310–3.
46. Shaffer K, Rosado-de-Christenson ML, Patz EF Jr, Young S, Farver CF. Thoracic lymphangioma in adults: CT and MR imaging features. Am J Roentgenol. 1994;162:283–9.